Shining Light on PAHs in Space

Andrews Mancilla, H.E.

4

The Path to PAHDs

We used a kinetic model to analyze the deuteration of PAHs over an astrophysically relevant PAH size range. Our specific goals were to understand how deuterium is locked in PAHs, and if PAHs can contribute to the deuterium fractionation problem at a significant level or not. We expanded the kinetic model of Andrews et al. (2016) to include reactions with deuterated species. The model calculates the abundances of PAHs and its fragments under the influence of photodissociation and atom addition reactions. It uses specific molecular properties for each PAH, based on the latest data available at the present time. It takes into account the small differences in the binding energy between CH and CD bonds which affects the photodissociation rates, as well as the differences in thermal velocity for atomic H and D that affects the addition reaction rate coefficient. Overall we find that deuteration of PAHs largely follows the atomic (D/H) ratio available in the gas phase. Thus the deuterium fractionation in PAHs will be higher if the (D/H) ratio in the ISM is higher. In that sense, the (D/H) ratio in PAHs is sensitive to its local conditions. Our results also show that the deuterium fractionation of PAHs with extra atoms in their edges (creating aliphatic sites) is higher than that of aromatic sites. We have compared our model results with recent observations of deuterated PAHs in photodissociation regions (PDRs). We conclude that the high deuteration observed implies that the gas phase reservoir must be highly fractionated, e.g., possibly because deep in clouds hydrogen is locked up in H_2 while deuterium can still be largely atomic. However, the implied atomic (D/H) fraction in the gas phase is much larger than what PDR models predict. Alternatively, the observed high deuterium fractionation on aromatic sites may reflect chemistry occurring in cold dense molecular cloud cores, that is preserved when (intermediate-to-large) PAHs are transported to the unshielded environment of PDRs. Such a model, can, however, not explain the observed high fractionation of the much more labile, aliphatic groups.

H. Andrews, A. Candian & A. G. G. M. Tielens
A&A, Submitted

4.1. Introduction

It is generally considered that all the deuterium in the universe was formed in the Big Bang (Epstein et al. 1976). The primordial (D/H) ratio is commonly estimated from observations of clouds in the line-of-sight towards distant quasars at high redshift (Adams 1976). Recent (D/H) values derived from observations of damped Lyman-α (DLA) systems, coupled with measurements of the angular power spectrum of the cosmic microwave background (CMB), agree on a cosmic D/H abundance of $\sim 2.5\times10^{-5}$ (Srianand et al. 2010; Coc et al. 2015; Cooke & Pettini 2016).

In theory, stars should completely destroy the deuterium in them (Mazzitelli & Moretti 1980), and therefore we expect the (D/H) abundance to decrease steadily as galaxies chemically evolve with time. However *Far-Ultraviolet Spectroscopic Explorer* (FUSE) observations revealed more puzzling results, showing considerable scatter in the (D/H) ratio in the local galactic disk (between ~ 0.5–2.2×10^{-5}; Linsky et al. 2006), with a value of 1.6×10^{-5} within the Local Bubble (Wood et al. 2004).

The values mentioned above cannot be accounted for solely by astration (Tosi 2010). Infall of unprocessed gas in the galaxy (Romano et al. 2006) and deuterium depletion onto dust grains (Draine 2004) have been proposed as important processes to explain the variation of the (D/H) ratio in the local galactic environment. Observationally, correlations of the (D/H) ratio with Fe, Si, and Ti depletions, and with the excitation temperature of molecular hydrogen suggest that deuterium depletion onto dust grains is important (Jura 1982; Draine 2004; Prochaska et al. 2005; Linsky et al. 2006). Theoretically, the slightly higher binding energy of the C-D bond over the C-H bond support the suggestion that carbonaceous grains could preferentially retain the D they acquire in their surface, leading to $(D/H)_{dust}/(D/H)_{gas}$ values as high as 5×10^4 (Draine 2006). For this same reason, polycyclic aromatic hydrocarbons (PAHs) may also be important reservoirs of D in space (Tielens 1997; Millar et al. 2000; Draine 2006).

Observational evidence for the presence of deuterated PAHs in the interstellar medium has been reported in few occasions (e.g., Peeters et al. 2004; Onaka et al. 2014; Doney et al. 2016). Given that deuterium is heavier than hydrogen, the PAH vibrational bands are expected to be slightly shifted to longer wavelengths, and –given the plethora of PAH bands at longer wavelengths– the signature of deuterated PAHs is better evaluated in the $4\,\mu$m region (analogue to the $3\,\mu$m region of –hydrogenated– PAHs). More specifically, PAHs with deuterium in them are expected to show bands at $4.4\,\mu$m (D in aromatic groups, analogue to the $3.3\,\mu$m) and 4.7–$4.8\,\mu$m (D in aliphatic groups, analogue to the 3.4–$3.5\,\mu$m bands) (Allamandola 1993; Bauschlicher et al. 1997; Hudgins et al. 2004). Peeters et al. (2004), using the *Infrared Space Telescope* (ISO), first reported the signature of deuterated PAHs in Orion. The observations led to $(D/H)_{PAH}$ ratios 10^4 times larger than the atomic (D/H) ratio found in the gas phase (Peeters et al. 2004; Draine 2006). More recently, Onaka et al. (2014) revisited these detections using the Infrared Camera (IRC) on board AKARI, and also observed the deuterium signature on PAHs, but estimated a $(D/H)_{PAH}$ lower than previously reported (< 0.03).

Extending this analysis to a larger sample, Doney et al. (2016) looked for the deuterated PAH signature in a sample of 53 H II regions using AKARI, out of which 41 were in the Milky Way. The footprint of deuterium in PAHs was found only in 6 sources, all in our Galaxy. Interestingly, it was found that in the few sources that presented the deuterated

PAH bands, C-D aliphatic bands were stronger than the C-D aromatic bands (contrary to what is observed with the C-H bands), meaning that the little amount of D attached to PAHs is preferably in an aliphatic group, rather than in an aromatic group (see also Peeters et al. 2004). They also observed a wide range of $(D/H)_{PAH}$ ratios, which points towards a $(D/H)_{PAH}$ ratio that is very sensitive to local physical conditions.

All these findings pose an interesting chemical question within the framework of interstellar PAHs. What physical conditions favor a high deuterium fractionation of PAHs? How sensitive is the $(D/H)_{PAH}$ ratio relative to the strength of the UV field and the atomic D and H densities? What fraction of the available D can be indeed locked in PAHs and in which form? In this work we will address these issues within the framework of the PAH kinetic model presented in Andrews et al. (2016). This model includes ionization/electron recombination of PAHs, multiphoton dissociation events, atomic addition reactions, and Eley-Rideal abstraction mechanism of aliphatic groups. We will consider the same PAHs as in Andrews et al. (2016), meaning the first three members of the *coronene family*. For these specific PAHs, many relevant molecular properties have been determined and they span an interesting PAH size range (between 24 and 96 carbon atoms). This will allow us to study how effective PAHs are in retaining the D attached to them.

The present work is organized as follows: section 4.2 presents a general overview of the kinetic model, and how reactions with deuterium are included. The results regarding the deuteration of PAHs, and how the $(D/H)_{PAH}$ varies with physical conditions for PAHs of different size are presented in section 4.3, and the implications of our results concerning the role of PAHs in the fractionation of D is discussed in section 4.4.

4.2. Method

4.2.1. PAH Structure

We use the PAH kinetic model of Andrews et al. (2016). This model only considered hydrogenation of PAHs. Therefore, modifications had to be made to include the deuteration of PAHs.

We consider 3 PAHs of increasing size within the *coronene family*: coronene $C_{24}H_{12}$, circumcoronene $C_{54}H_{18}$, and circumcircumcoronene $C_{96}H_{24}$. These species span the range of astrophysically relevant PAH sizes (Allamandola et al. 1989), and they are expected to be among the most stable PAHs in the ISM (Ricca et al. 2012). Coronene has a carbon core with 12 H atoms attached in pairs to 6 different rings (i.e., 6 duo rings). Circumcoronene has 12 H atoms attached in pairs to 6 separate rings (6 duo rings), and 6 H atoms attached to other 6 peripheral rings (6 solo rings). Circumcircumcoronene has similarly 6 duo rings and 12 solo rings.

Each PAH is characterized by the total number of edge atoms $N_{edge} = N_H + N_D$, where N_H is the total number of H atoms attached at their periphery, and N_D the total number of D atoms attached at their periphery. We refer to homogenic PAHs as those having either only H atoms ($N_D = 0$) or only D atoms ($N_H = 0$). Heterogenic PAHs are those having both H and D atoms in a given ratio (also referred as PAHDs). Those PAHs with all outer edge C atoms occupied are referred to as the normal molecules, i.e., molecules having the

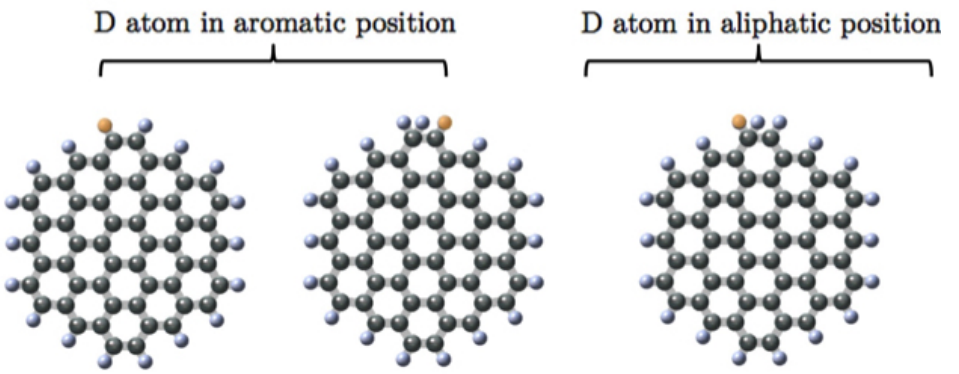

Figure 4.1: Position of a deuterium atom in circumcoronene derivatives. Here we consider molecules with only 1 D atom as an example of heterogenic species. Carbon cores are depicted in grey, H atoms are depicted in white, and D atoms are depicted in orange. From left to right we see $C_{54}H_{17}D$, and two isomers of $C_{54}H_{18}D$. The $C_{54}H_{17}D$ molecule has the D atom in an aromatic position. The heterogenic molecules with $N_{edge} = 19$ on the other hand, can have an HH aliphatic group while keeping the D atom in an aromatic position; or can have an HD aliphatic group, while having only H atoms in aromatic positions.

total number of edge atoms $N_{edge} = N_H^0$, where $N_H^0 = 12$, 18 and 24 for coronene, circumcoronene and circumcircumcoronene, respectively. Species with $0 < N_{edge} < N_H^0$ are called partial species, while those having $N_{edge} > N_H^0$ are in super states.

For the sake of simplicity, we consider that these PAHs can vary their edge occupation (i.e., total number of edge atoms) from being completely devoid of edge atoms ($N_H = 0$ and $N_D = 0$) to having up to 2 extra edge atoms (i.e., $N_{edge} = N_H^0 + 2$). We limit ourselves to super states of only +2 as this reduces the number of isomers. Given that the larger molecules are not usually found in highly de-hydrogen/deuterated partial states, we also consider that D atoms can only be attached to the duo rings of the PAHs, that is, all solo rings have only H atoms in them. Thus, the smallest deuterated species for coronene, circumcoronene and circumcircumcoronene are $C_{24}D$, $C_{54}H_6D$ and $C_{96}H_{12}D$, respectively. Both these choices are also supported by the IR studies and neither of these choices has an important impact on our results, but they considerably speed up the computing time.

For the upcoming analysis it is important to keep in mind then that for partial species with $N_{edge} > N_{solo}$, deuterium atoms are attached to an aromatic position (see Figure 4.1); while for species in super states deuterium can be attached to either an aromatic position or an aliphatic position (Figure 4.1). Regarding ionization states, we considered anions (Z = -1), neutrals (Z = 0) and cations (Z = 1). Other states are not relevant under the physical conditions we probe.

4.2.2. Molecular Properties

We use the molecular characteristics described in Andrews et al. (2016). Given the lack of specific molecular properties for deuterated species, we decided to use the properties of the homogenic hydrogenated species in Andrews et al. (2016) for all (deuterated and heterogenic) isomers with the same number of edge atoms. This includes the ion-

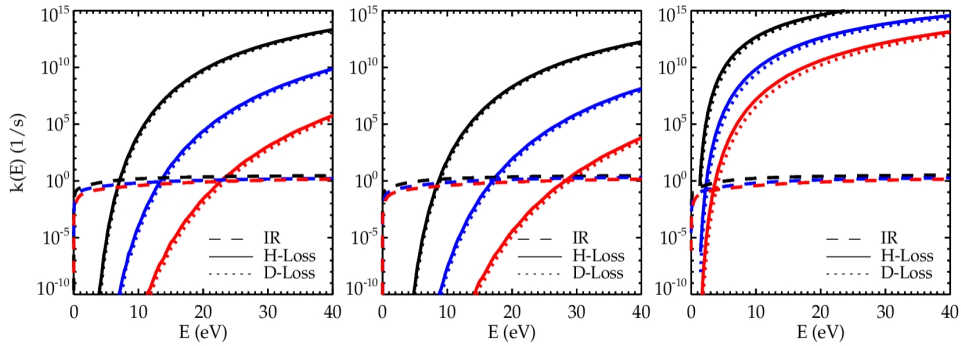

Figure 4.2: Comparison of the IR emission and photodissociation rates for H and D losses as a function of internal energy of the PAHs. The rates determined for coronene, circumcoronene and circumcircumcoronene derivatives are shown in black, blue and red, respectively. The left panel shows the rates for the PAHs in partial states with a total number of edge atoms $N_{edge} = N_H^0 - 1$, where N_H^0 is the number of edge atoms of the PAHs in their normal state (i.e., 12 for coronene, 18 for circumcoronene and 24 for circumcircumcoronene). We have plotted these to exemplify the rates for molecules with an odd number of edge atoms. The middle panel shows the rates for the normal state molecules, exemplifying also the rates for PAHs with an even number of edge atoms. The right panel shows the rates for the first super-state molecules (i.e., with $N_{edge} = N_H^0 + 1$) to illustrate the rates for super-state PAHs.

ization potentials (IP) and electron affinities (EA) (i.e., the inverse linear relation between these energies and the edge occupation of each PAH), ionization yields, UV absorption cross sections, polarizabilities, IR cross sections and density of states.

4.2.3. Reactions with Deuterium

As mentioned before, Andrews et al. (2016) included ionization and electron recombination of PAHs, (multiphoton) H and H_2 dissociation processes, reactivity with H, and Eley-Rideal abstraction of H_2 from superhydrogenated species. Here, we include PAH reactivity with D, direct D-loss through photodissociation, and Eley-Rideal abstraction of D_2 and HD from species in super states. It is important to mention that we will not consider H_2 photodissociation, since this process will hardly compete against H and D losses in the environments sampled in this work (Andrews et al. 2016).

Photodissociation

Photodissociation rates of H-loss are calculated using the same activation energies and entropies as in Andrews et al. (2016). For species in partial states we then consider activation energies of E_{act} = 4.6 and 4.1 eV, and entropies of ΔS = 44.8 and 55.6 J/K/mol, for species having an even and odd number of edge atoms, respectively (and for all charge states admitted in the model). In order to calculate the photodissociation rate of D-loss from species in partial states, we modified the energies taking into account the different zero-point energies of C-H and C-D bonds (i.e., 0.09 eV). This value comes from a comparison between the ZPE of CH_4 and CD_4 molecules using calculations at the B3LYP/4-31G level. No scaling was applied to the ZPE to account for anharmonicity.

Figure 4.2 shows a comparison of the IR emission and the photodissociation rates as a function of internal energy of hydrogenated PAHs. This illustrates that there are only minor differences in the resulting H and D-loss rates over the relevant energy range.

We consider that the partial species first lose all the edge atoms in duo rings. For PAHs with an even number of edge atoms we include a term in the estimation of the j-loss rate, to account for the number of H and D atoms in each molecule:

$$\widetilde{k}_j = \frac{N_{j,duo}}{(N_{edge} - N_{solo})} k_j \tag{4.1}$$

where k_j is the loss rate given by expression (7) in Andrews et al. (2016); and $N_{j,duo}$ corresponds to the total number of j atoms in duo rings that the PAH can lose. For PAHs with an odd number of edge atoms we consider $\widetilde{k}_j = k_j$ since the PAH will lose the edge atom left alone in the duo ring. Once all edge atoms in duos are stripped off the PAH, then the molecule starts losing the solo H-atoms with $E_{act} = 4.6$ eV, and change in entropy of $\Delta S = 44.8$ J/K/mol (see more in Andrews et al. 2016).

Regarding PAHs in super states, for the H-loss we adopt the binding energies of an extra H-atom in a duo position, which are of 1.4 eV for the anion, 1.4 eV for the neutral and 1.55 eV for the cation, and an activation entropy of 55.6 J/K/mol (Bauschlicher & Ricca 2014). For the D-loss we again consider the 0.09 eV difference in the activation energy with respect to the values used for the H-loss (Figure 4.2). We assume extra H and D atoms always stick to duo positions for all molecules. For PAHs with an even number of edge atoms we also include a term in the estimation of the photodissociation rate of j-loss, to account for the number of H and D atoms in aliphatic groups:

$$\widetilde{k}_j = \frac{N_{j,alip}}{(N_{H,alip} + N_{D,alip})} k_j \tag{4.2}$$

where in this case, $N_{H,alip}$ and $N_{D,alip}$ correspond to the total number of H and D atoms in aliphatic groups, respectively. For PAHs with an odd number of edge atoms we consider $\widetilde{k}_H = k_H$ in case the PAH has a H_2 left; $\widetilde{k}_D = k_D$ in case the PAH has a D_2 left; and $\widetilde{k}_H = 0.5\times k_H$ and $\widetilde{k}_D = 0.5\times k_D$ in case the PAH has an HD left.

Figure 4.3 shows the variation of the D-loss rates with G_0 for the heterogenic species with $N_D = 1$ and $N_{edge} = N_H^0 - 1$, N_H^0, and $N_H^0 + 1$. Regarding partial and normal species, we see that for coronene single-photon events dominate, while for the larger PAHs multiphoton events take place. For PAHs in super states on the other hand, due to the low activation energies, single-photon events dominate for all species. These results are very much in line with those obtained for the corresponding H-loss rates, since the energy differences between C-D and C-H bonds are small.

Addition Rates

For positively ionized species we consider the H addition rate derived from the experiments of Le Page et al. (1997) on the hydrogenation of coronene, that is a rate of 1.4×10^{-10} cm^3/s (see Andrews et al. 2016). We use this rate for all positively ionized species and for all N_{edge} states. For D addition we divide this rate by a factor of $\sqrt{m_D/m_H} \sim 1.4$ to take into account the slightly larger mass of the D atom, m_D, over that of the H atom, m_H.

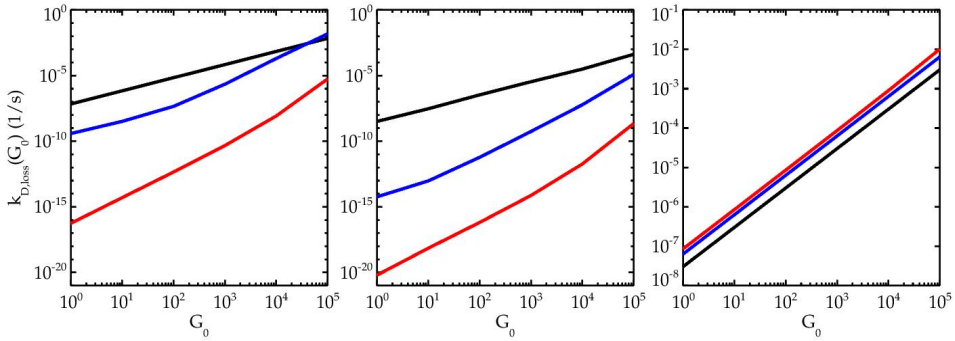

Figure 4.3: Deuterium loss rates through photodissociation as a function of the intensity of the UV field, G_0. These rates are the resulting one considering also the H-loss and IR emission as relaxation channels. The rates are shown for neutral heterogenic molecules with 1 D atom in their edges. The black curves refer to coronene molecules, while the blue and red curves refer to circumcoronene and circumcircumcoronene molecules respectively. The left panel shows the D-loss rates for the partial-state PAHs $C_{24}H_{10}D$, $C_{54}H_{16}D$ and $C_{96}H_{22}D$, with the D atom alone in a duo ring. As in Figure 4.2 we have plotted these to exemplify the rates for molecules with an odd number of edge atoms. The middle panel shows the rates for the heterogenic normal molecules (i.e., $N_{egde} = N^0_H$): $C_{24}H_{11}D$, $C_{54}H_{17}D$ and $C_{96}H_{23}D$. The right panel shows the rates for the heterogenic molecules in the first super-state with an HD aliphatic group: $C_{24}H_{12}D$, $C_{54}H_{18}D$ and $C_{96}H_{24}D$. For coronene molecules the rates scale linearly with G_0, while for the larger species multiphoton events are important for the normal and partial derivatives. The D-loss rate for the super-state molecules on the other hand, changes linearly with G_0 for all species.

For neutral PAHs we use the geometrical cross sections of each molecule, σ_{geom}, together with the energy barriers given by Rauls & Hornekær (2008) for the H addition to neutral coronene:

$$k_{j,add} = \sigma_{geom} \sqrt{\frac{8\, k_B\, T_{gas}}{\pi\, m_j}} \exp(-E_{barrier}/k_B/T_{gas}), \tag{4.3}$$

where k_B is the Boltzmann constant; T_{gas} is the gas temperature; $E_{barrier}$ is the energy barrier for the addition; and m_j is the mass of the j atom reacting with the PAH. For super states we consider the energy barriers from Rauls & Hornekær (2008) for both H and D addition. For the partial species we do not consider any barriers ($E_{barrier} = 0$), and we adopt a 7% efficiency as found for cations by Demarais et al. (2014). The H and D addition reactions to anionic PAHs on the other hand, is considered as a dissociative attachment process (Demarais et al. 2012). That is, the H addition rate is $7.8{\times}10^{-10}$ cm^3/s. Again for the D addition rate we divide by a factor of ~ 1.4 to account for the different atomic masses, which leads to a D addition rate of $5.5{\times}10^{-10}$ cm^3/s for anionic molecules.

It is important to keep in mind that for PAHs in super states, we must consider the edge atoms each PAH has prior to the atom addition, since this determines whether there will be an H_2, HD or D_2 new aliphatic group in the PAH. To include this, we consider an extra factor in the reaction rate given by $P_j = N_{j,duo}/(N_{H,duo} + N_{D,duo})$, where $N_{H,duo}$

Table 4.1: Physical conditions used in the model.

Model	G_0 (Habing units)	n (cm^{-3})	n_D (cm^{-3})
Diffuse Cloud	1	500	0.016
PDR	1000	10^6	16

and $N_{D,duo}$ correspond to the number of aromatic H and D atoms in duos prior to any additions, respectively. Thus, for example, the PAH $C_aH_bD_c$ with an HD aliphatic group will form from the H addition to the corresponding isomer(s) of the PAH $C_aH_{b-1}D_c$, where the reaction rate is given by $P_D(C_aH_{b-1}D_c) \times k_{H,add}(C_aH_{b-1}D_c)$; and it will form from the D addition to the corresponding isomer(s) of the PAH $C_aH_bD_{c-1}$, where the rate is given by $P_H(C_aH_bD_{c-1}) \times k_{D,add}(C_aH_bD_{c-1})$.

Abstraction Rates

We consider the same parameters for the H_2 abstraction as in Andrews et al. (2016). Given the lack of data, we use the same parameters for the abstraction of H_2, D_2 and HD. The cross section used comes from experiments on the deuteration of coronene, and corresponds to a value of 0.06 $Å^2$ (Mennella et al. 2012). We consider the first abstraction as a barrierless process, and the second abstraction as involving a 0.01 eV barrier (Bauschlicher & Bakes 2001; Rauls & Hornekær 2008). The only difference between the rates comes from the mass of the atom colliding with the PAH.

Just like for the addition processes to PAHs in super states, we include a term of the form $P_j = N_{j,alip}/(N_{H,alip} + N_{D,alip})$, to consider the atom (in an aliphatic group) that the colliding atom is more likely to abstract. When a j atom collides with an HD aliphatic group, we consider it is equally likely to abstract the H as to abstract the D. We assume this since we expect the energy difference to be insignificant.

4.3. Results

We consider two different environments where the total density, n, and the intensity of the UV radiation field, G_0, are kept fixed, while the density of atomic H, n_H, is varied (see Table 4.1). For the first run we considered $G_0 = 1$ and a total density of 500 cm^{-3} (to simulate a diffuse cloud in the ISM such as ζ Oph), while for the second run we considered a $G_0 = 1000$ and total density of 10^6 cm^{-3} (relevant for a PDR environment). We adopted a $(D/H)_{ISM}$ ratio of 1.6×10^{-5}, and therefore the D density remains fixed at 0.016 cm^{-3} and 16 cm^{-3} for the first and the second runs respectively.

We chose to perform two runs because the edge occupation distribution of PAHs, $f(N_{edge})$, depends on the available H (and D) but also on the ionization balance, which at any given G_0/n_H ratio varies for different values of G_0 and n (this is because our IP and EA values depend on the edge occupation of each molecule).

4.3.1. Relative Abundance Distribution of PAHs

Figure 4.4 shows the total edge occupation distribution of each PAH for the two runs. For the diffuse ISM run ($G_0 = 1$, $n = 500$ cm^{-3}) we show the results for the larger molecules (circumcoronene and circumcircumcoronene), while for the PDR model ($G_0 = 1000$, $n = 10^6$ cm^{-3}) we show the results for the smaller species (coronene and circumcoronene). As seen from the Figure, PAHs of different sizes show different $f(\mathrm{N_{edge}})$ distributions. At a given G_0/n_H we see the smallest molecule, coronene, stripped off of all edge atoms (black curve), while the larger molecules –as they are more difficult to dissociate– are overall in normal to super states. There is some contribution from partial states for the intermediate PAH, circumcoronene, at $G_0/n_H = 1$ (second run) but is $< 1\%$. For the largest PAH, circumcircumcoronene, there are no partial species.

Comparing top and bottom panels, at higher G_0 and n values the transition from partial to normal and super states occurs at slightly higher G_0/n_H ratio (grey dashed lines). This shift is due to the difference in the $f(Z)$ distribution between the two runs, which is itself given by the IP($\mathrm{N_{edge}}$) and EA($\mathrm{N_{edge}}$) relations we adopted. At a given G_0/n_H ratio, there is a larger fraction of anions in the second run than in the first one. For example, for circumcoronene at $G_0/n_H = 0.002$ the charge state of PAHs is $f(\text{-}1) \simeq 50\%$, $f(0) \simeq 50\%$, and $f(1) \simeq 0.2\%$ in the first run, while in the second run the fractions are $f(\text{-}1) \simeq 68\%$, $f(0) \simeq 32\%$, and $f(1) \simeq 0.07\%$. Similarly, at $G_0/n_H = 1$ in the first run, $f(\text{-}1) \simeq 69\%$, $f(0) \simeq 30\%$ and $f(1) \simeq 0.1\%$, while in the second run the relative contributions are $f(\text{-}1) \simeq 82\%$, $f(0) \simeq 18\%$, and $f(1) \simeq 0.04\%$. Since anions have higher addition rates, the transition from PAHs with less to more edge atoms happens at a higher G_0/n_H in the second run. This is valid for all species. For coronene, the transition from $\mathrm{N_{edge}} = 0$ to partial species occurs at $G_0/n_H \simeq 0.0025$ in the first run, and at $\simeq 0.004$ in the second run; the transition for circumcoronene molecules from (mostly) normal to super states occurs at $G_0/n_H \simeq 0.004$ in the first run, and at $\simeq 0.005$ in the second run; while the transition for the largest PAH occurs at $G_0/n_H \simeq 0.0035$ and $\simeq 0.004$, for the first and second run respectively.

Aside from the shift, the behaviour of the $\mathrm{N_{edge}}$ distribution is similar between both runs. Small PAHs are rarely found in normal and super states because they are more prone towards dissociation, and therefore we see coronene as a carbon cluster for a wide range of G_0/n_H ratios. As n_H increases, so does $\mathrm{N_{edge}}$. Up to $\mathrm{N_{edge}} = 8$ the distributions $f(\mathrm{N_{edge}})$ are rather symmetrical with respect to the G_0/n_H given by the grey line in each panel. The distribution of partial species with $\mathrm{N_{edge}} \geq 9$ are different. This is because of the IP/EA dependence on $\mathrm{N_{edge}}$. For coronene, PAHs with less than $\mathrm{N_{edge}} = 8$, have electron sticking coefficients s_{e^-} higher than 0.9, which leads to higher electron recombination rates than for PAHs with more edge atoms. Therefore the PAHs with lower $\mathrm{N_{edge}}$ will tend to electron recombine more, and as mentioned before, anions in our models have higher H and D addition rates than neutrals. For $\mathrm{N_{edge}} \geq 9$ electron sticking coefficients are < 0.5, and therefore the electron recombination rates are severely decreased compared to those of smaller PAHs (e.g., with $s_{e^-} \sim 1$ the electron recombination rates are 2.4 times higher than the rate with $s_{e^-} \sim 0.4$, and $\sim 10^4$ times higher than for normal coronene which has an $s_{e^-} = 7.8{\times}10^{-5}$). Once there are normal molecules, the H and D attachment rates are the same for all Z, since we use the barriers from Rauls & Hornekær (2008). These barriers determine the distribution of the super states where the first addition has a barrier, while the second does not (see $\mathrm{N_{edge}} = 13$ and 14 distributions).

For circumcoronene and circumcircumcoronene, EA > 1 eV and thus $s_{e^-} = 1$, leading to the same electron recombination rates for all N_{edge}. Thus, for the larger molecules, the $f(N_{edge})$ distributions are symmetrical relative to G_0/n_H (grey lines).

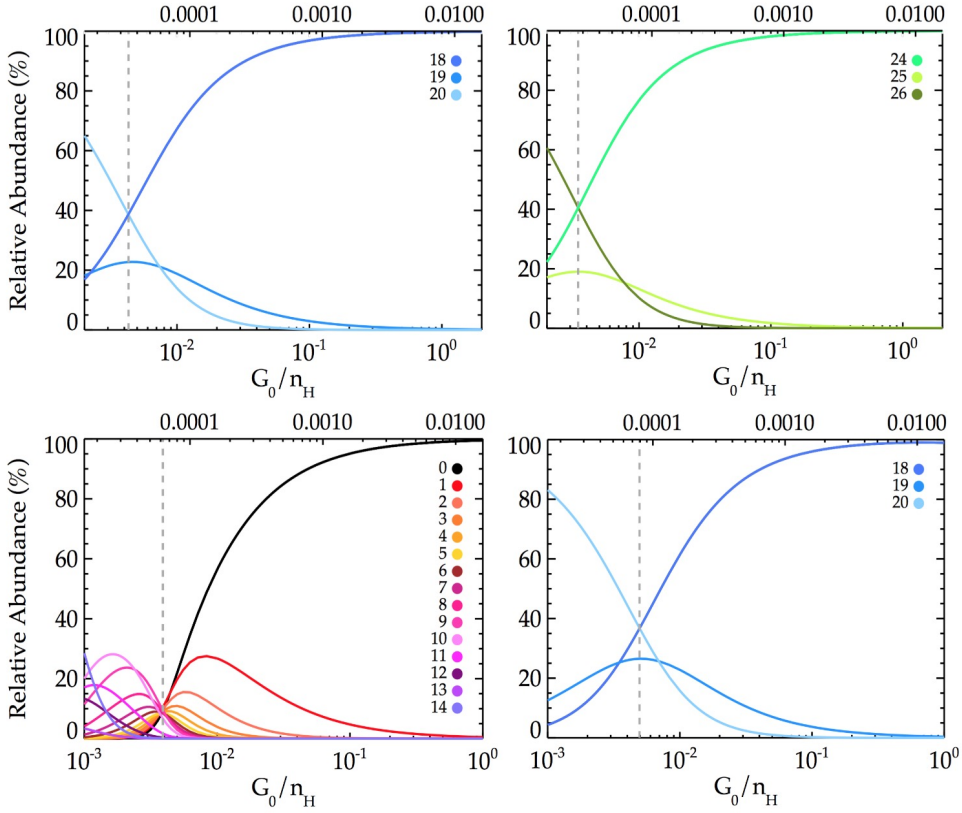

Figure 4.4: Relative abundance of PAHs with a number of edge atoms N_{edge} as a function of G_0/n_H. Each curve considers the sum of the relative abundance of all charge states for each species. The top panels show the distribution $f(N_{edge})$ for circumcoronene (left) and circumcircumcoronene (right) in the first run, where we considered $G_0 = 1$ and a total density $n = 500$ cm^{-3}, illustrating a diffuse ISM type of environment (Table 4.1). The bottom panels show the distribution of coronene (left) and circumcoronene (right) derivatives for the second run, where we considered $G_0 = 1000$ and total density $n = 10^6$ cm^{-3}, exemplifying a more PDR-like environment. The grey dashed lines indicate the G_0/n_H at which the large species, circumcoronene and circumcircumcoronene derivatives, change from normal to super states; while coronene derivatives change from being completely devoid of edge atoms (i.e., C_{24}, black curve) to higher occupation states. The top axis shows the atomic n_D/n_H density ratio. In general, results are similar between the two runs (hence we do not show the results for coronene derivatives in the first run, nor for circumcircumcoronene molecules in the second run). The main difference is in the transition points, which occur at slightly higher G_0/n_H in the second run. This shift in the transition points is related to variations in the charge state distribution of the species (read text).

4.3.2. Deuterium Content in PAHs

Regarding the deuteration of PAHs, while coronene can hold only 1 D atom in its edge, the larger PAHs can hold up to 2 (although PAHs with 1 D atom always dominate the heterogenic species). Most of the PAHs will be homogenic, containing only H atoms in their edges. Homogenic species containing only D are only found for coronene as $C_{24}D$. For coronene, more partial species can only survive in highly shielded environments, where the difference between n_H and n_D is large enough to overcome the fact that when dissociating it will be more likely for the PAH to lose an H rather than a D atom (coronene species will have 1 D only). The larger molecules on the other hand, will always be heterogenic.

Figure 4.5 shows the (D/H) ratio for the three PAH species. Coronene derivatives are mostly completely dehydrogenated for most of the G_0/n_H range in both runs: C_{24} represents about 99.8% of the population at $G_0/n_H = 2$ in the first run, and 99.5% of the population at $G_0/n_H = 1$ in the second run. The (D/H) for coronene molecules then is given by $[C_{24}D]/[C_{24}H]$. This ratio is basically determined by the addition rates of atoms to the C_{24} molecule: $k_{D,add}/k_{H,add} \propto (n_D/n_H)\times\sqrt{(m_H/m_D)}$, which is lower than the n_D/n_H available in the medium by a factor of $\sqrt{2} \sim 1.4$ (dashed grey line in Figure 4.5). This relation is valid down to $G_0/n_H \sim 0.005$–0.006, where species with $N_{edge} > 1$ atoms start increasing their abundance $> 40\%$. In this new regime, the (D/H) ratio which is given by $\sum_{n=1}^{N}[C_{24}H_nD]/\sum_{m=1}^{N+1}(m[C_{24}H_m])$ (where the sum runs over all N_{edge} relevant at a given G_0/n_H ratio) can be approximated by $[C_{24}H_nD]/((n+1)[C_{24}H_{n+1}])$ where $n + 1 = N_{edge}$ that dominates the mixture.

From Figure 4.5 we see there is a dip in the (D/H) ratio for coronene. This dip appears once partial species start dominating the mixture. Even more, we notice that the slope of the dip is steeper when the species with low N_{edge} appear, and becomes flatter as species with higher N_{edge} come into play. This happens because the formation and destruction mechanisms vary for molecules with significantly different N_{edge}. These mechanisms add extra terms to the expressions for the D and H content in coronene species. Since H-only molecules are far more abundant than the heterogenic species, these extra terms become even more relevant for the H-only species, which in turn makes the (D/H) ratio lower than $n_D/(\sqrt{2}\,n_H)$, which is the factor valid at high G_0/n_H ratios.

We saw that at high G_0/n_H ratios (D/H) = $[C_{24}D]/[C_{24}H]$, where the formation of $C_{24}D$ is given by the D addition to C_{24}, and the formation of $C_{24}H$ by the H addition to the C_{24} molecule (destruction mechanisms are similar for both species). In more shielded environments on the other hand, heterogenic species with 1 D (i.e. $C_{24}H_nD$) are mainly formed by the H addition to the $C_{24}H_{n-1}D$ molecules, and not due to the D addition to H-only PAHs. This is because of the increasing difference between n_H and n_D at lower G_0/n_H ratios (e.g., differences greater than 10^4 at $G_0/n_H < 0.005$ in the second run). Regarding H-only species, coronene molecules with $N_{edge} \leq 4$ are mainly formed by the H addition to anions (and ionization of anions). Partial coronene PAHs with $5 \leq N_{edge} \leq 8$ are formed not only by the H addition to anions, but also from the loss of H atoms from the $N_H + 1$ molecules. Larger species with $N_{edge} = 9$–12, will be formed by those same processes, plus the H addition to neutrals since these molecules do not easily recombine with electrons. Also the destruction rates for these species are slightly lower than for the molecules with lower N_{edge} (which are mainly destroyed by electron recombination). Notice that the decrease in the (D/H) ratio relative to the $n_D/(\sqrt{2}\,n_H)$ relation in Figure 4.5 (right panel) becomes the largest once species with $N_{edge} = 9$ and 10 atoms become important. This is also the point where the

slope of the dip starts flattening. This happens because for these species, even though we are adding formation processes, such increase is not dramatic because H addition to neutrals is slower than for anions. For the second run, at the lowest G_0/n_H ratio super state species become as relevant as N_{edge} = 10 and 11 species. For these molecules, the destruction rates are higher than for the partial species, but also the formation rates are higher. Therefore as we go to more shielded environments, the change in the (D/H) ratio is not as steep as for high G_0/n_H ratios where PAHs with less N_{edge} atoms dominate the mixture.

For the larger species the situation is different than for coronene. For both circumcoronene and circumcircumcoronene, the distribution of species is dominated by the normal molecule at high G_0/n_H ratio, and by super states in more shielded environments. Hence, we see again the same dip as for coronene, but extending throughout a wider G_0/n_H range, since these molecules are more likely to be found in their normal states rather than in partial states. At high G_0/n_H ratio the (D/H) mainly follows the $[C_{54}H_{17}D]/(18[C_{54}H_{18}])$ ratio in the case of circumcoronene, and $[C_{96}H_{23}D]/(24[C_{96}H_{24}])$ for circumcircumcoronene. As mentioned above, these larger molecules can hold 2 D atoms in them (even 3 but at relative abundances $\sim 10^{-8}$%), but their contributions will not dominate the (D/H) ratio. At G_0/n_H = 1 in the second run, considering circumcoronene molecules with N_{edge} = 17–19, the contribution from $C_{54}H_nD$ species is $\simeq$0.3%, while $C_{54}H_nD_2$ species are $\simeq 6\times10^{-4}$%. Similarly, for circumcircumcoronene, considering PAHs with N_{edge} = 24–26, those with 1 D atom contribute $\simeq$ 0.09%, while species with 2 D atoms contribute $\simeq 4\times10^{-5}$%. We notice that the contribution from heterogenic species is slightly larger for circumcoronene than for circumcircumcoronene derivatives. This is because the H and D addition processes are dominated by anions for both species (i.e., we do not consider the cross sections of the PAHs for these rates) and because –as mentioned before– there are slightly more neutrals for circumcircumcoronene in normal to super states, which have lower addition rates than the anionic population.

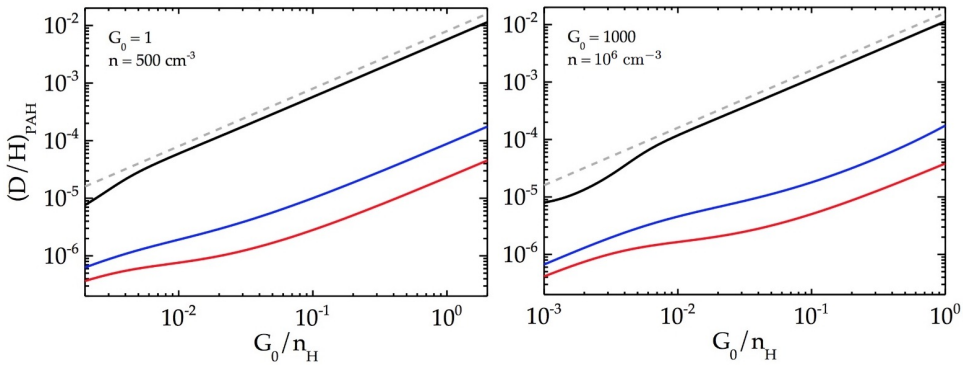

Figure 4.5: Variation of the (D/H) ratio in PAHs as a function of G_0/n_H. Here we use the same color scheme as in Figure 4.2. The left panel shows the results for the first run (diffuse ISM), and the right panel shows the results for the second run (PDR). The dashed grey lines indicate the n_D/n_H variation. As seen from the Figure, the variation of the (D/H) ratio for each PAH is similar between both runs. The difference is in the fact that in the second run we go further down to a G_0/n_H = 0.001, and thus, we see the molecules going into the super-state regime.

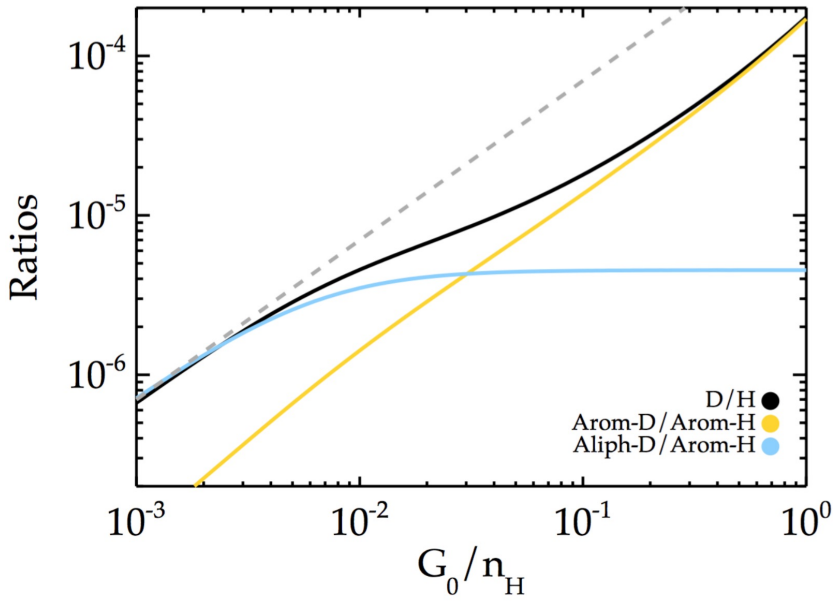

Figure 4.6: Comparison of the aromatic and aliphatic D relative to the aromatic H content of circumcoronene derivatives at $G_0 = 1000$ and $n = 10^6$ cm^{-3}. The total (D/H) ratio in circumcoronene molecules is shown in black, while the dashed grey line is the $n_D/(\bar{m}\ \sqrt{2}\, n_H)$ relation, with $n_D = 16$ cm^{-3} and $\bar{m} = 16.2$, the weighted average number of aromatic H atoms in circumcoronene derivatives at $n_H = 10^6$ cm^{-3}. Here we see the (D/H) ratio in circumcoronene molecules follows the (arom-D/arom-H) relation at high G_0/n_H, while in more dense environments it follows the (aliph-D/arom-H) ratio which is proportional to the $n_D/(\bar{m}\ \sqrt{2}\, n_H)$ relation at the lowest G_0/n_H considered.

The formation of circumcoronene and circumcircumcoronene molecules in normal states will be affected not just by the addition processes, but also by the fast dissociation of molecules in super states. The (D/H) ratio then follows the aromatic ratio, (arom-D/arom-H), as long as the normal species dominate the mixture (see Figure 4.6). Once super state molecules become more abundant, the (D/H) ratio starts approaching the aliphatic-D over aromatic-H ratio, (aliph-D/arom-H), which follows $n_D/(\sqrt{2}\, n_H\, \bar{m})$, where $\bar{m}$ is the average number of H atoms in aromatic modes in super state molecules weighted by their respective contributions (e.g., at $G_0/n_H = 0.001$ for $G_0 = 1000$, $\bar{m} = 16.2$ and 22.3 for circumcoronene and circumcircumcoronene, respectively). If we were to extend this further to more dense environments, we would see the curve reaching the $n_D/(16\ \sqrt{2}\, n_H)$ and $n_D/(22\ \sqrt{2}\, n_H)$ limit for circumcoronene and circumcircumcoronene derivatives respectively, as the population would be fully dominated by the maximum N_{edge} adopted in our calculations.

Figure 4.7 shows the variation of the aromatic and aliphatic-D content in super state derivatives of circumcoronene and circumcircumcoronene species. From here we see that heterogenic PAHs in super states have more aliphatic than aromatic D at $G_0/n_H < 0.01$ in a diffuse cloud environment, and at $G_0/n_H < 0.02$ in a PDR-like environment. At high G_0/n_H ratios there is more aromatic D than aliphatic D simply because the normal molecules dominate the population of PAHs (increasing the aromatic D-content).

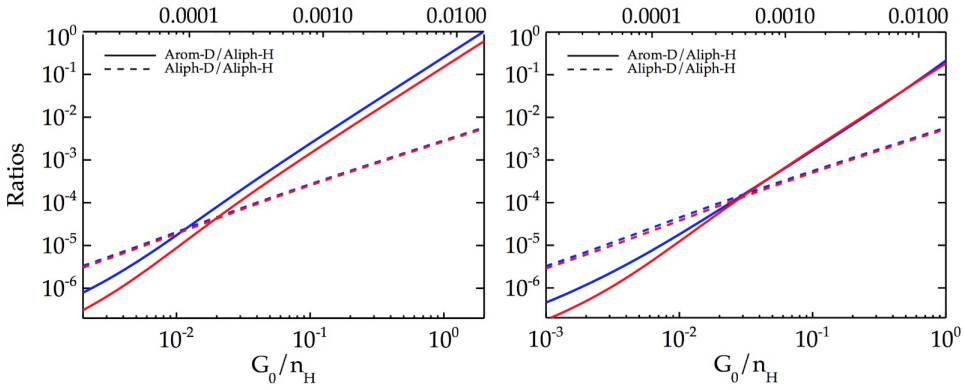

Figure 4.7: Variation of the aromatic and aliphatic D relative to the aliphatic H content in PAHs. Again we use the same color scheme as in Figure 4.5. The left panel shows the results for the first run (diffuse ISM), and the right panel shows the results for the second run (PDR). The top axis shows the atomic n_D/n_H density ratio. PAHs in super states will have the D (mostly 1 D) preferably in an aliphatic mode rather than in an aromatic mode. This happens even when comparing isomers of equal N_{edge} at high G_0/n_H ratios. However at high G_0/n_H ratios, molecules in normal state contribute greatly to the amount of aromatic D. Therefore we see (arom-D/aliph-H) > (aliph-D/aliph-H) down to a G_0/n_H of a few times 0.01. That is the point where addition processes overcome the large dissociation rates adopted for super-state molecules, and species with $N_{edge} = N_H^0 + 2$ start to appear. The shift in this transition point between both runs is related to the different charge state distributions, as explained for the results of Figure 4.4.

The (aliph-D/aliph-H) follows the ratio between the D and H addition rates to normal (and super state) molecules. Since we use the same barriers for D and H additions, (aliph-D/aliph-H) $\propto n_D/(\bar{m}\ \sqrt{2}\, n_H)$ where $\bar{m}$ is the average number of aliphatic H atoms in super-state molecules, weighted by their corresponding abundance (e.g., for circumcoronene $\bar{m}$ = 2 at G_0/n_H = 1, and $\bar{m}$ = 3.54 at G_0/n_H = 0.001 in the PDR run). PAHs with aliphatic D (i.e., HD aliphatic group) will be mainly formed by the D addition to H-only normal PAHs. When facing photon absorption at high G_0/n_H ratios, these molecules will preferably lose the H atom (about 3 times more often than the D), retaining the D atom in an aromatic position. However, once addition processes overcome the high dissociation rates for super states (at $G_0/n_H \sim 0.01$; see Figure 4.7), the more likely thing to happen is that the molecules will add another H atom, forming species with HD and HH aliphatic groups.

Heterogenic species with only aliphatic H (i.e., with aromatic D) are mainly formed from the H addition to other heterogenic species. For example, $C_{54}H_{18}D$ with an HH aliphatic group, will be formed from the H addition to the $C_{54}H_{17}D$ molecule. This occurs at a lower rate than the formation of $C_{54}H_{18}D$ with an HD aliphatic group, since H only species (i.e., $C_{54}H_{18}$ molecules) are about 300 times more abundant than $C_{54}H_{17}D$ at G_0/n_H = 1 in the PDR run. This 300 factor compensates the fact that the H addition rate is about $(n_D/(\sqrt{2}\, n_H))^{-1} \sim 88$ times greater than the D addition rate, and also the fact that in order to create an HH aliphatic group, the H atom can be added to 11/12 positions (we assume aliphatic groups are in duo rings only). Therefore even though $n_H > n_D$, H only molecules are so abundant, that more aliphatic D will be created after the first addition to the normal PAHs. Once we go into lower G_0/n_H ratios, the more likely thing to happen to the molecules with an HH aliphatic group is to attach another H to the available position, which most of

the times will be another H. Only once in a while the new H will fall on the aromatic D contributing again to the formation of molecules with HH-HD aliphatic groups.

According to our results –and assuming the three PAHs studied here are good representatives of PAHs of different sizes– small species have higher (D/H) ratios than larger ones, even though larger species can hold more than 1 D per molecule, while small PAHs hold only 1 D atom in their edges. This is partly because in larger species there are more edge positions to be occupied by (mostly H) atoms, and partly because, due to the PAH size difference, at a given G_0/n_H ratio larger species are mainly found in their normal (and super) state and therefore having about N_H^0 (mostly H) atoms, while smaller PAHs like coronene are found as completely dehydrogenated with small traces of $N_{edge} = 1$ molecules.

4.4. Discussion

4.4.1. Deuterium fractionation of PAHs

The largest $(D/H)_{PAH}$ ratios are attained by coronene molecules. However it should be noted that under the conditions probed here, coronene molecules are mostly C_{24} clusters, which may be rapidly destroyed in the ISM. From that perspective, we ignore coronene in the subsequent discussion (it was mainly included in our calculations to illustrate the trends with PAH size). From Figures 4.5, 4.7 and 4.8, we see that the behaviour of the (D/H) ratio with G_0/n_H is similar between the two runs (diffuse cloud vs the PDR-like environment). The main difference is given by the n_D/n_H ratio, that will shift the curves upwards or downwards depending on the atomic D relative to the atomic H available in the gas phase. As we have adopted a constant elemental abundance ratio of $(D/H)_{ISM} = 1.6\times10^{-5}$, we can take the variation in G_0/n_H as the variation of the H/H_2 ratio in the gas phase. Our results show that the (D/H) ratio in the PAHs reflects the (D/H) ratio in the reservoir. As the reservoir is never very highly fractionated in our calculations, the (D/H) ratio of the PAHs is dominated by the species where one H atom has been replaced by a D.

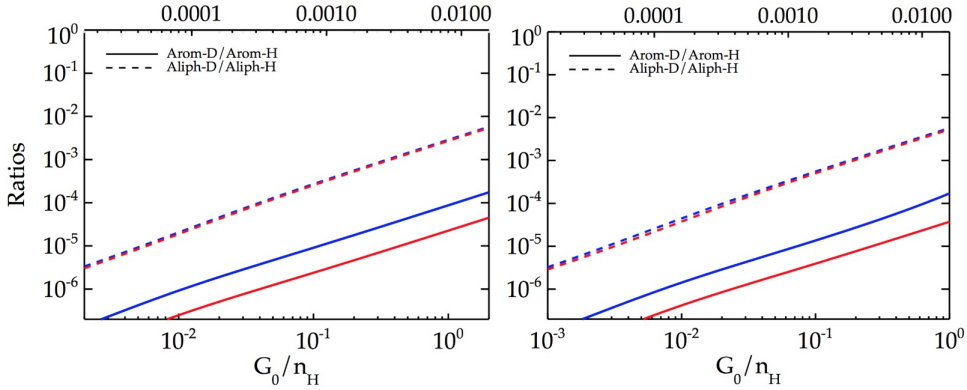

Figure 4.8: Variation of the (arom-D/arom-H) and (aliph-D/aliph-H) ratios for circumcoronene and circumcircumcoronene. Again we use the same color scheme as in Figure 4.5. The left panel shows the results for the first run (diffuse ISM), and the right panel shows the results for the second run (PDR). The top axis shows the atomic n_D/n_H density ratio. Here we see that for both runs and both PAH species, the aliphatic (D/H) ratio is greater than the aromatic (D/H) ratio for all G_0/n_H ratios considered in the model (see more in the discussion).

The atomic (D/H) ratio can be much larger in the diffuse ISM and in PDRs, as H_2 is well protected against photo-destruction through self-shielding, while the photo-destruction of HD is dominated by dust shielding. As a result, photo-destruction of HD is important far deeper into a cloud or PDR than H_2. This is counteracted by additional HD formation not available to H_2. As for H_2, HD can be formed on grain surfaces, but for diffuse clouds –once some H_2 is present– the dominant formation route of HD is $D^+ + H_2 \rightarrow H^+ + HD$ (Black & Dalgarno 1973; Le Petit et al. 2002). In warm, dense PDRs, HD can also be formed efficiently by the direct reaction, $D + H_2 \rightarrow H + HD$, which has an activation barrier of 3820 K. Still, models show photo-destruction wins, leading to an enhancement of the atomic (D/H) ratio by up to a factor of 100 (Le Petit et al. 2002). Hence, deuterium fractionation of PAHs is predicted to be modest in diffuse clouds and in PDRs.

Much higher deuterium fractionations of interstellar molecules ($\simeq 10^{-2}$) have been observed for molecules such as HCO^+ and HCN inside dark clouds (Lis et al. 2002). Observations of hot Corinos associated with low mass protostars have also revealed deuterium fractionations of the order of $\simeq 1$, and even the presence of multiply deuterated species (Ceccarelli et al. 2007). The deuterium fractionation of these species has been ascribed to H and D atoms reacting with CO and other species on grain surfaces, during a cold dense phase of the evolution of the cloud. After evaporation of the ices, these fractionation effects "live on" for some 10^4 yr in the warm gas, before gas phase chemistry "equilibrates" the deuterated species with the local physical conditions (Charnley et al. 1997). The high deuterium fractionation of H_3^+ can reach levels where H_2D^+, HD_2^+, and even D_3^+ are more abundant than the parent species when the main destruction agent, CO, depletes in ices in these cores (Roberts et al. 2003). As PAHs are expected to be the last ones to deplete in ices inside dense cores (as their thermal velocity is a factor of $\simeq 5$ less than for CO), reactions of the type $H_2D^+ + PAH \rightarrow H_2 + PAHD^+$ could drive deuterium fractionation of PAHs to very high levels (Tielens 1992). Further deuteration may also occur if PAHs are accreted into ice mantles; e.g., due to photolysis (Sandford et al. 2000).

Once the core dissolves, ices evaporate, and the material finds itself in the PDR surface or in the diffuse ISM, the highly deuterium-enriched PAHs will "equilibrate" with the local physical conditions. The timescale for this depends on the PAH size, the binding energy involved, and the strength of the local radiation field. As Figure 4.3 illustrates, for a 100 C-atom PAH, the aromatic (D/H) ratio acquired in a dense core could survive over the lifetime of a PDR (10^4 yr) for a radiation field of $G_0 < 10^4$. In contrast, a 50 C-atom PAH cannot be exposed to a radiation field stronger than $G_0 \simeq 10^2$ without losing its deuterium signature. In the diffuse ISM, both species will retain their high deuterium fractionation in the aromatic modes over relevant timescales (Figure 4.3). Because of the much lower binding energies, aliphatic groups will much more quickly return to the gas phase (steady state) fractionation value. Even for a large PAH, the timescale is $\simeq 1$ yr in the diffuse ISM.

4.4.2. Observations of interstellar PAHDs

Due to the difference in reduced mass, the C-D vibrational transitions of deuterated PAHs are shifted to longer wavelengths than the corresponding C-H modes. In particular, the aromatic C-D stretching mode (the counterpart of the 3.3 μm aromatic C-H stretching mode) occurs at 4.4 μm, while aliphatic C-D stretching modes are at 4.6–4.8 μm (analogue to the C-H bands at 3.4–3.5 μm). The 4–5 μm region is a relatively clean region of the spectrum with no strong aromatic bands. The longer wavelength in- and out-of-plane bending modes of deuterated bonds also shift but into regions which are crowded with other PAH

bands. Weak bands at 4.4 and 4.6 μm have been detected in a few bright PDRs/H II regions, and have been ascribed to deuterated PAHs (Peeters et al. 2004; Onaka et al. 2014; Doney et al. 2016). It should be noted that these observations are very difficult, as the bands are very weak and –at the limited spectral resolution of these studies– corrections for atomic lines are challenging. The results show that only a small fraction (6 out of 53) of the sources show these bands (Doney et al. 2016). The implied deuterium fractionation for these sources ranges from 0.03[1] up to 0.4 (Doney et al. 2016). In addition, the results show that the aliphatic (D/H) ratio is higher than the aromatic (D/H) ratio, with the aliphatic (D/H) ratio varying from 0.1 to 1 for the detected sources (Doney et al. 2016).

Our calculations show that, in steady state, the deuterium fractionation in PAHs is directly related to the atomic (D/H) ratio in the gas. At an atomic (D/H) ratio of 10^{-2}, the calculated aromatic (D/H) ratio is only 10^{-4} while the aliphatic (D/H) ratio is 10^{-3} (Figure 4.8). In order to reach an aliphatic (D/H) ratio of 0.1 –the lowest value in the observed ratios– a gas phase atomic (D/H) ratio well above 0.1 is needed. Such a high atomic (D/H) ratio in the gas phase is at variance with models for PDRs. In agreement with the observations, our models do predict that PAHs in super states are substantially more deuterated than the purely aromatic molecules. However there is another issue somewhat "hidden" here: the presence of $\simeq 10\%$ super-state-PAHs requires a $G_0/n_H \simeq 0.03$ (Andrews et al. 2016). If the atomic (D/H) ratio in the gas phase is 0.1, this implies a total density of $n \simeq 2{\times}10^5\, G_0$ which for a PDR with $G_0 = 10^3$ would imply a density of $2{\times}10^8$ cm^{-3}. Thus, the presence of a high abundance of D in super states requires a very dense but moderate UV field environment, and such conditions are untypical for PDRs. We note that this is a direct consequence of the low binding energy of the super states. As emphasized by Andrews et al. (2016), this low binding energy makes the appearance of the 3.4 μm band very unlikely. The current result on deuteration reinforces this point. Methyl groups provide an alternative interpretation for the 3.4 μm band. Now, the aliphatic H in CH_3 groups is bound by $\simeq 3.7$ eV, and hence this H (or D) is much less labile under irradiation by strong UV fields. The (photo)chemistry of methyl groups is not well understood as the formation of a tropylium structure is involved (Zhen et al. 2016; Rapacioli et al. 2015). Reaction of this structure with atomic H (or D) back to a methyl group may well be inhibited by an activation barrier. We intend to come back to this issue in a future study, once the chemical pathways involved are better characterized.

4.4.3. PAHs and the gas phase abundance of D

The observed variations in the gas phase (D/H) ratio in the solar neighbourhood (10–20 ppm; Draine 2006; Onaka et al. 2014) suggest the presence of a substantial reservoir of deuterium that is not traced by atomic D nor molecular HD. Deuterated PAHs –as well as deuterated dust grains– are expected to be that reservoir (Linsky et al. 2006; Draine 2006). The observed fraction of the elemental C locked up in PAHs is $\simeq 10\%$ or 35 ppm. With a typical aromatic (H/C) ratio for PAHs of 1/4–1/3, this implies $\simeq 10$ and $\simeq 20$ ppm of aromatic and aliphatic sites, respectively, that could be deuterated. Hence, for PAHs to make a substantial contribution to the missing D reservoir, the D fractionation of PAHs in the diffuse ISM would have to be very high. Focusing again on the astrophysically relevant size range of 50–100 C-atoms, atomic (D/H) ratios in the gas phase would have to be close to unity for this to occur (cf., Fig. 4.5). The IR observations of PDRs and H II regions suggest that the amount of D in PAHs represents 10 ppm of the elemental D (Doney et al. 2016). For the

[1] Close to the detection limit of this study

diffuse ISM, we do not have direct, IR observations of the deuterium fractionation of PAHs. However, the atomic (D/H) column density is directly measured by Copernicus and FUSE and is low for the sight-lines investigated by Linsky et al. (2006). Thus, if PAHs are indeed an important contributor to the missing D problem, then this deuterium fractionation must be a relict from an earlier phase of the evolution, where the PAHs were in an environment characterized by a high gas phase (D/H) ratio. As Figure 4.3 illustrates, D fractionation of the aromatic sites can be preserved against photochemical destruction for a timescale ranging from a few million years for 50 C-atom PAHs, to as long as the PAH survives for a 100 C-atom PAH.

As discussed in section 4.4.1, our models do not reproduce the high implied D fractionation of PAHs in PDRs. But then, on a galactic scale, very little of the ISM cycles often through PDRs. PAHs could then acquire a high D fractionation in the shielded environment of cold dense cores (e.g., through either reactions with the deuterated isotopic isomers of H_3^+ in the gas phase), so that the deuterium fractionation observed in PDRs would be derived from this type of environment. Such process could potentially explain the observed substantial variations in the gas phase (D/H) ratio, as different sight-lines might probe different histories of the material.

4.5. Conclusions

We used a kinetic model to analyze the abundance of deuterium in PAHs. We considered 3 PAHs of different size, between 24 and 96 carbon atoms, all within the *coronene* family. We modelled two different environments of fixed total density and intensity of the incident UV radiation field. The two models are expected to represent the diffuse ISM and a PDR-like environment.

Overall we find that deuteration of PAHs is scarce, and its variation with G_0/n_H is similar between the two runs for a PAH of a given size. Clear differences do appear for the different PAH sizes. At a given G_0/n_H, the smallest molecule is stripped off of all edge atoms, while the larger molecules are found in higher degrees of edge occupation (entering to the regime where aliphatic bonds are present). This is what rules the deuteration degree of the PAHs. This also leads to higher (D/H) ratios in small PAHs than in the larger species. However small PAHs are not expected to survive and hence they are not expected to be a relevant reservoir of deuterium.

Regarding the role of PAHs in the deuterium fractionation problem, we find that the (D/H) ratio in PAHs follows the (D/H) ratio available in the reservoir. Given our assumptions, the PAHs studied here cannot reach the fractionation values necessary to account for the observed variations in the (D/H) of the ISM. Our study instead suggests that PAHs between 50 and 100 carbon atoms could eventually reach high fractionation values in more shielded environments (low G_0/n_H), where the available (D/H) might be way larger than what we assumed here. The aromatic (D/H) ratio acquired by a large PAH in a dense core could survive over a time of $\sim 10^4$ yr before losing its deuterium signature when exposed to a more intense UV radiation field in a PDR. In a diffuse ISM-type of environment, even a 50 carbon atom PAH could retain its aromatic deuterium. However, in both cases the aliphatic signature is more easily lost because of the low dissociation energy of an aliphatic CD bond. From this, we also conclude that the deuterated aliphatic signature at 4–5 μm observed in PDRs/H II regions is most likely not due to deuterated PAHs, as modelled in

this work. In view of its larger binding energy, aliphatic D associated with methyl groups might be more resistant against photo-destruction in high UV fields, but the chemistry of such groups in the ISM is not well understood yet. Further laboratory studies will be required to elucidate the molecular structures resulting from their photodissociation and their re-hydrogenation/re-deuteration processes.

Future observations with the upcoming JWST are expected to bring new insights on the deuteration level of PAHs. We recognize that, in PDRs, deuteration might be particularly relevant for deeper, UV-poor environments where excitation of the bands might be less likely. Nevertheless, the expected supreme sensitivity of JWST may make these bands and the chemistry they trace detectable. Of course, high deuteration levels inherited from a cold dense core phase could survive well into the PDR and be readily detected by JWST.

Acknowledgements

Studies of interstellar PAHs at Leiden Observatory are supported through advanced ERC grant 246976 from the European Research Council, through a grant by the Dutch Science Agency, NWO, as part of the Dutch Astrochemistry Network, and through the Spinoza premie from the Dutch Science Agency, NWO. Computing time has been made available by NWO (project SH-362-15) and calculations were performed at the Cartesius supercomputer (SurfSARA, Science Park, Amsterdam NL). A.C. acknowledges NWO for a VENI grant (639.041.543). We also acknowledge the European Union (EU) and Horizon 2020 funding awarded under the Marie Sklodowska-Curie action to the EUROPAH consortium, grant number 722346.

Bibliography

Adams, T. F. 1976, A&A, 50, 461
Allamandola, L. J. 1993, in Astronomical Society of the Pacific Conference Series, Vol. 41, Astronomical Infrared Spectroscopy: Future Observational Directions, ed. S. Kwok, 197
Allamandola, L. J., Tielens, A. G. G. M., & Barker, J. R. 1989, ApJS, 71, 733
Andrews, H., Candian, A., & Tielens, A. G. G. M. 2016, A&A, 595A, 23A
Bauschlicher, C. W., & Bakes, E. L. O. 2001, Chem. Phys., 274, 11–14
Bauschlicher, Jr., C. W., Langhoff, S. R., Sandford, S. A., & Hudgins, D. M. 1997, The Journal of Physical Chemistry A, 101, 2414
Bauschlicher, C. W., & Ricca, A. 2014, Theo. Chem. Acc., 133, 1454
Black, J. H., & Dalgarno, A. 1973, ApJ, 184, L101
Ceccarelli, C., Caselli, P., Herbst, E., Tielens, A. G. G. M., & Caux, E. 2007, Protostars and Planets V, 47
Charnley, S. B., Tielens, A. G. G. M., & Rodgers, S. D. 1997, ApJ, 482, L203–L207
Coc, A., Petitjean, P., Uzan, J.-P., Vangioni, E., Descouvemont, P., Iliadis, C., & Longland, R. 2015, Phys. Rev. D, 92, 123526
Cooke, R., & Pettini, M. 2016, MNRAS, 455, 1512–1521
Demarais, N. J., Yang, Z., Martinez, O., Wehres, N., Snow, T. P., & Bierbaum, V. M. 2012, AJ, 746, 32
Demarais, N. J., Yang, Z., Snow, T. P., & Bierbaum, V. M. 2014, ApJ, 784, 25
Doney, K. D., Candian, A., Mori, T., Onaka, T., & Tielens, A. G. G. M. 2016, A&A, 586, A65
Draine, B.T. 2004, in Origin and Evolution of the Elements, ed. A. McWilliams & M. Rauch (Cambridge: Cambridge Univ. Press), p. 320
Draine, B. T. 2006, ASPC, 348, 58
Epstein, R. I., Lattimer, J. M. & Schramm, D. N. 1976, Nature, 263, 198
Hudgins, D. M., Bauschlicher, Jr., C. W., & Sandford, S. A. 2004, ApJ, 614, 770
Jura, M. 1982, in Advances in UV Astronomy: 4 Years of IUE Research, ed. Y. Kondo, J. M. Mead, & R. D. Chapman (NASA CP 2238: Greenbelt, MD: NSAS), 54
Le Page, V., Keheyan, Y., Bierbaum, V. M., & Snow, T. P. 1997, JACS, 119, 35

Le Petit, F., Roueff, E., & Le Bourlot, J. 2002, A&A, 390, 369
Linsky, J. L., Draine, B. T., Moos, H. W., et al. 2006, ApJ, 647, 1106
Lis, D. C., Gerin, M., Phillips, T. G., & Motte, F. 2002, ApJ, 569, 322
Mazzitelli, I. & Moretti, M. 1980, ApJ, 235, 955
Mennella, V., Hornekær, L., Thrower, J., & Accolla, M. 2012, ApJ, 745, L2
Millar, T. J., Roberts, H., Markwick, A. J., & Charnley, S. B. 2000, Philos. Trans. R. Soc. London A, 358, 2535
Onaka, T., Mori, T. I., Sakon, I., et al. 2014, ApJ, 780, 114
Peeters, E., Allamandola, L. J., Bauschlicher, Jr., C. W., et al. 2004, ApJ, 604, 252
Prochaska, J. X., Tripp, T. M., & Howk, J. C. 2005, ApJ, 620, L39
Rapacioli, M., Simon, A., Marshall, C.C.M., Cuny, J., Kokkin, D., Spiegelman, F., & Joblin, C. 2015, J. Phys. Chem. A, 119, 12845–12854
Rauls, E., & Hornekær, L. 2008, ApJ, 679, 531
Ricca, A., Bauschlicher, C. W., Jr., Boersma, C., Tielens, A. G. G. M., & Allamandola, L. J. 2012, ApJ, 754, 75
Roberts, H., Herbst, E., & Millar, T. J. 2003, ApJ, 591, L41
Romano, D., Tosi, M., Chiappini, C., & Matteucci, F. 2006, MNRAS, 369, 295
Sandford, S. A., Bernstein, M. P., Allamandola, L. J., Gillette, J. S., & Zare, R. N. 2000, ApJ, 538, 691
Srianand, R., Gupta, N., Petitjean, P., Noterdaeme, P. & Ledoux, C. 2010, MNRAS, 405, 1888
Tielens, A. G. G. M. 1992, in IAU Symposium, Vol. 150, Astrochemistry of Cosmic Phenomena, ed. P. D. Singh, 91
Tielens, A. G. G. M. 1997, in AIP Conf. Proc. 402, Astrophysical Implications of the Laboratory Study of Presolar Materials, ed. T. H. Bernatowicz & E. K. Zinner (New York: AIP), 523
Tosi, M. 2010, in Proc. IAU Symp. 268, Light Elements in the Universe, ed. C. Charbonnel, M. Tosi, F. Primas & C. Chiappini (Cambridge: Cambridge Univ. Press), 153
Verstraete, L., Puget, J. L., Falgarone, E., et al. 1996, A&A, 315, L337
Wood, B. E., Linsky, J. L., Hébrard, G., Williger, G. M., Moos, H. W., & Blair, W. P. 2004, ApJ, 609, 838
Junfeng, Z., Castellanos, P., Linnartz, H. & Tielens, A. G. G. M. 2016, Molecular Astrophysics, 5, 1–8